

Enhancing the oscillatory Unruh effect with a dense cloud of accelerating photodetectors

Hui Wang¹ and Miles Blencowe¹

¹*Department of Physics and Astronomy, Dartmouth College, Hanover, New Hampshire 03755, USA*

We consider $N \gg 1$ oscillating (i.e. accelerating) center of mass photodetectors modeled as two level systems (TLS) that are coupled to a microwave cavity mode, and solve for the average photon number production from vacuum in the presence of cavity and detector damping. The accelerating photodetector-cavity system maps onto a parametrically driven Dicke-type model and when the TLS detector number N exceeds a critical value, the photon production undergoes a phase transition from a normal phase to a superradiant-like, inverted lasing phase in which the average photon number is significantly enhanced such as to be potentially measurable. As one possible realization, we consider a mechanical membrane with a dense concentration of nitrogen-vacancy (NV) center defects undergoing GHz flexural motion, and contained within a 3D, superconducting microwave cavity.

The Unruh effect (UE) predicts that the Minkowski vacuum state appears as a thermal state with temperature $T = \hbar a / (2\pi c k_B)$ for a noninertial, uniformly accelerating photodetector [1]. For example, a 1 K thermal photon bath requires a photodetector acceleration of $a = 2.47 \times 10^{20}$ m/s², which seems impossibly high for any current or planned tabletop experiments. One possible way to enhance the UE is to place an accelerating photodetector within an electromagnetic cavity [2]. The finite confining volume then necessitates a non-uniform, e.g., oscillatory acceleration [3]. While such a non-uniformly accelerating detector might not ‘see’ a thermal photon spectrum, there nevertheless remains the predicted phenomenon of photon detection from the vacuum due to the non-inertial motion of the detector. For oscillatory acceleration, we term this the ‘oscillatory Unruh effect’.

In recent work [4, 5], we proposed close analogs of the oscillatory UE that involve coplanar (i.e., 2D) superconducting microwave cavity circuit systems [6]. The photodetector was modelled alternatively as a harmonic oscillator [4] and as a qubit [5] that capacitively couple to the 2D cavity via a mechanically oscillating film bulk acoustic resonator (FBAR) [7]; by increasing the FBAR capacitor plate area, a strong detector-cavity coupling can be achieved. Furthermore, when the FBAR mechanical frequency resonantly matches the sum of the cavity mode and detector ground-first excited energy level splitting, the photon production rate from cavity vacuum is resonantly enhanced [2] so as to be detectable. The use of an FBAR introduces an actual mechanical acceleration, in contrast to previous UE analogs where the accelerating photodetector is mimicked by an electromagnetically induced, time changing detector coupling [8, 9].

In contrast to the progress made towards analogs, a feasible way to demonstrate the *genuine* oscillatory UE where the photodetectors are accelerating within a 3D electromagnetic cavity (as opposed to the above 2D analogues) is still lacking. In this letter, we describe a possible way to realize the oscillatory UE with a scheme that involves $N \gg 1$ pointlike, two level system (TLS) accelerating photodetectors contained within a microwave cavity (Fig. 1). The TLS detectors are assumed to be embedded within a membrane undergoing small, GHz flexural vibrations (i.e. displacements normal to the membrane surface). As we shall show, beyond a certain critical detector number the photon production from vacuum is coherently enhanced, resulting in superradiant-like bursts of light [10, 11] that may be detectable.

We consider the following model Hamiltonian for the cavity-TLS detectors system in the rest frame of the

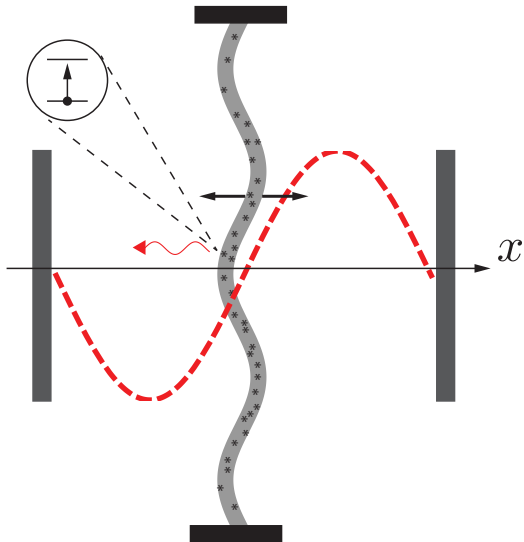


FIG. 1: Oscillatory UE scheme. The membrane located at $x = L/2$, midway between cavity wall (mirror) boundaries at $x = 0, L$, undergoes flexural vibrations in the x -coordinate direction, resulting in the oscillatory acceleration of pointlike, TLS photodetectors embedded within the membrane.

cavity [8]:

$$H = \hbar\omega_c a^\dagger a + \hbar\omega_{d0} \sum_{i=1}^N \frac{d\tau_i}{dt} \frac{\sigma_i^z}{2} + \hbar\lambda_0 \sum_{i=1}^N \frac{d\tau_i}{dt} \sin[k_c A \cos(\Omega_m t + \phi_i)] (a + a^\dagger) \sigma_i^x, \quad (1)$$

where we assume a single mode approximation for the cavity electromagnetic radiation (see below) with mode frequency $\omega_c = ck_c = 2\pi c/L$, and L the cavity length. The TLS detectors are assumed to have identical center of mass rest frame transition frequencies ω_{d0} and coupling strength λ_0 between each detector's internal degrees of freedom and the cavity mode. With the membrane undergoing driven (e.g., piezoelectrically actuated) flexural oscillations at some frequency Ω_m about the midway point $x = L/2$ of the cavity, the center of mass of the i th detector follows the trajectory $x_i(t) = L/2 + A \cos(\Omega_m t + \phi_i)$, where A is the detector oscillation amplitude and ϕ_i the oscillation phase. We assume that the cavity mode field is uniform in the transverse y - z directions coinciding also with the static, equilibrium membrane surface so that the TLSs all have approximately the same coupling strength λ_0 with the cavity mode field.

Hamiltonian (1) accounts for relativistic time dilation through the presence of the reciprocal Lorentz factors $d\tau_i/dt = \sqrt{1 - \xi^2 \sin^2(\Omega_m t + \phi_i)}$, where $\xi = \Omega_m A/c$, and may be thought of as a relativistic, parametrically driven Dicke model [12, 13]. However, with membrane flexural, microwave scale frequencies $\Omega_m \sim 2\pi \times 10$ GHz and achievable oscillation amplitudes $A \sim 10^{-10}$ m, we have $\xi \sim 10^{-8}$ and hence the time dilation factors can be safely neglected for potential laboratory realizations. The sinusoidal interaction term can then be well-approximated as $\sin[k_c A \cos(\Omega_m t + \phi_i)] \approx k_c A \cos(\Omega_m t + \phi_i) = \omega_c A/c \cos(\Omega_m t + \phi_i)$. Nevertheless, from a theoretical standpoint it is still interesting to work with the relativistic Hamiltonian

(1), and allow also for relativistic TLS accelerations in exploring photon production when starting initially with the TLSs in their ground states and the cavity in its vacuum state.

We now obtain a much simpler Hamiltonian by approximating (1) [14]; the validity of the various approximations will be given below. Setting the phases $\phi_i = 0$, we can describe the collection of N TLSs as a single $N + 1$ -level system viewed as a large pseudospin vector of length $j = N/2$, with the collective spin operators given by $J^z \equiv \sum_{i=1}^N \sigma_i^z/2$ and $J^\pm \equiv \sum_{i=1}^N \sigma_i^\pm$. Expanding the time-dependent terms in Eq. (1) and keeping only terms up to second harmonics in Ω_m , the TLSs' transition frequency is renormalized as $\omega_d = \omega_{d0}D_0$ and with an additive frequency modulation $\omega_{d0}D_2 \cos(2\Omega_m t)$, where D_0 and D_2 are ξ -dependent constants [14]. Imposing the resonance condition $\Omega_m = \omega_c + \omega_d$, we then transform the frequency renormalized, modulated Hamiltonian to the rotating frame via the unitary $U_{\text{RF}}(t) = \exp(i\omega_c a^\dagger a t + iJ^z [\omega_d t + \omega_{d0}D_2 \sin(2\Omega_m t)/2\Omega_m])$. Applying the rotating wave approximation (RWA), the resulting approximate Hamiltonian is

$$H \approx \hbar\lambda(a^\dagger J^+ + aJ^-), \quad (2)$$

where the coupling constant is $\lambda = \frac{1}{2}\lambda_0 C_1 [J_0(\omega_{d0}D_2/2\Omega_m) - J_1(\omega_{d0}D_2/2\Omega_m)]$, with C_1 a ξ , Ω_m -dependent constant [14], and $J_0(z)$, $J_1(z)$ are Bessel functions of the first kind.

Assuming the cavity mode and TLSs to be coupled to independent environments, we model the cavity-TLSs system dynamics with a Lindblad master equation

$$\dot{\rho} = -\frac{i}{\hbar}[H, \rho] + \gamma_c \mathcal{L}_a[\rho] + \gamma_d \sum_{i=1}^N \mathcal{L}_{\sigma_i^-}[\rho], \quad (3)$$

where γ_c and γ_d are the cavity and TLS energy damping rates, respectively, and the Lindblad superoperator is defined as $\mathcal{L}_A[\rho] \equiv A\rho A^\dagger - \frac{1}{2}A^\dagger A\rho - \frac{1}{2}\rho A^\dagger A$; we assume the environment temperature to be small compared to the frequencies of the cavity mode and TLSs, and also assume that each TLS has approximately the same damping rate.

In order to test the validity of the approximate Hamiltonian (2), the master equation (3) was solved numerically for the average photon number, considering both Hamiltonians (1) and (2) in the case of a few TLSs. The single cavity mode approximation in Hamiltonian (1) is justified provided the approximate resonance condition $\Omega_m \approx \omega_c + \omega_d$ is satisfied [4]. This resonance condition also justifies the RWA Hamiltonian (2), provided $|\lambda| \ll \omega_c, \omega_d$. Furthermore, even for relativistic motions with $\xi \lesssim 1$, using the approximate Hamiltonian (2) in the master equation provides an accurate description of the average photon number dynamics. Finally, numerical simulations suggest that the average photon number dynamics is relatively insensitive to the phase ϕ_i -dependencies of the TLSs center of mass motions. From now on, we will use Hamiltonian (2) in the master equation (3).

One approach to solving this master equation begins with the Holstein-Primakoff (H-P) transformation $J^+ = b^\dagger \sqrt{2j - b^\dagger b}$, $J^- = \sqrt{2j - b^\dagger b} b$, which maps the collective spin operators J^\pm to the bosonic creation and annihilation operators b^\dagger , b [15]. In the large $j = N/2$ limit, the collective spin of the N TLSs is approximated as a single harmonic oscillator, with Hamiltonian (2) mapped to $\hbar\sqrt{N}\lambda(a^\dagger b^\dagger + ab)$. This coincides with the RWA Hamiltonian that was used in Ref. [4] to describe the oscillatory UE for a system comprising a photodetector coupled to a cavity electromagnetic field in the single mode approximation, with the detector's internal degrees of freedom modeled as a harmonic oscillator, and the oscillator detector's center of mass oscillating at a frequency Ω_m that matches the sum of the cavity frequency and detector internal frequency. This system describes a nondegenerate parametric amplification process, with cavity-detector photon pairs produced from the vacuum via mechanical pumping. Including cavity and detector damping and solving analytically the corresponding master equation for the above bosonic Hamiltonian, the

average cavity photon number in the long time limit is $\langle a^\dagger a \rangle = 4\gamma_d N \lambda^2 / (\gamma_c + \gamma_d)(\gamma_c \gamma_d - 4N\lambda^2)$. Note that the system exhibits a parametric instability when the effective coupling strength $\sqrt{N}\lambda$ exceeds the value $\sqrt{\gamma_c \gamma_d}/2$. While such an instability indicates a breakdown of the above H-P derived approximation method, it does point to the possible existence of an enhanced vacuum photon production phase for $N > N_{\text{crit}} = \gamma_c \gamma_d / (4\lambda^2)$ in the original cavity-TLSs model dynamics given by equations (1–3), where there is no such instability.

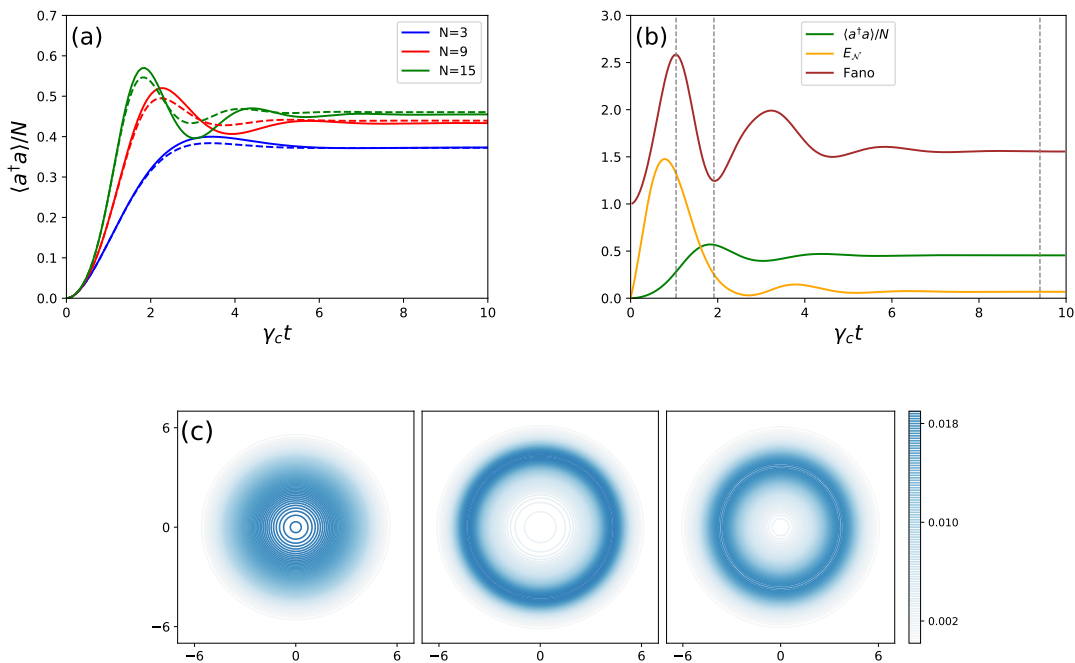


FIG. 2: (a) Dynamical evolution of $\langle a^\dagger a \rangle / N$; solid lines are the numerical solutions and dashed lines are the cumulant expansion approximation. (b) Evolution of $\langle a^\dagger a \rangle / N$, Fano factor, as well as the entanglement (logarithmic negativity $E_{\mathcal{N}}$) for $N = 15$ case; the vertical dashed lines indicate the approximate time instants corresponding to the Wigner function snapshots appearing in (c). The parameters are $\gamma_c = \gamma_d = 0.02$ Hz and $\lambda = 0.01$ Hz, corresponding to $N_{\text{crit}} = 1$.

In Fig. 2a, we show for some example, illustrative parameters corresponding to $N_{\text{crit}} = 1$, the dynamical behavior of the average scaled cavity photon number $\langle a^\dagger a \rangle / N$ starting from the cavity mode vacuum and with all the TLSs initially in their ground states at time $t = 0$. The solid line plots are obtained by numerically solving [16] the Lindblad master equation (3) with the RWA Hamiltonian (2); the utilized numerical method exploits the permutation symmetry of the density operator [17], which reduces the size of the Hilbert space required for the TLSs and increases the accessible value of N up to around 20, depending on the parameter choices. The dashed line plots are obtained by solving approximate equations for the non-vanishing first and second order moments derived from the master equation (3) [18, 19]; we employ an improved cumulant expansion approximation [14] that involves setting fourth order cumulants to zero instead of third order cumulants. In particular, with each of the TLSs giving an identical contribution to the moment equations, we can replace $\sigma_i^z, \sigma_i^\pm \sigma_j^z$ ($i \neq j$) with $\sigma_1^z, \sigma_2^\pm \sigma_1^z$ respectively. Utilizing the identity

$\sigma_1^z = 2\sigma_1^+\sigma_1^- - 1$ and approximating that the fourth cumulants vanish, we obtain for example the following non-vanishing third moment approximation [14]: $\langle a^\dagger \sigma_2^+ \sigma_1^z \rangle = \langle a^\dagger \sigma_2^+ \rangle \langle \sigma_1^z \rangle + 2\langle a^\dagger \sigma_1^+ \rangle \langle \sigma_1^- \sigma_2^+ \rangle$; note that the latter approximation contains an additional term involving products of second moments as compared with the usual, third cumulant vanishing approximation [18, 19].

As N increases above N_{crit} , a ‘burst’ peak of cavity photon production from vacuum appears in Fig. 2a that progressively grows in magnitude, narrows, and shifts to earlier times. Furthermore, the long time limit steady state average photon number grows in magnitude. These features qualitatively resemble those of Dicke superradiance [10, 11], although in the latter process the TLSs are initially prepared in their excited state and the cavity in the ground state. In order to get a better idea of the cavity mode-TLSs state, in Fig. 2b we show for $N = 15$ the time dependence of the logarithmic negativity entanglement measure $E_{\mathcal{N}}$ [20] between the cavity and TLS ensemble and also the cavity Fano factor $(\langle (a^\dagger a)^2 \rangle - \langle a^\dagger a \rangle^2) / \langle a^\dagger a \rangle$ in comparison with the average scaled cavity photon number. The entanglement grows and reaches a maximum roughly when the Fano factor is a maximum, while the entanglement is relatively small, although non-zero, in the long-time limit. This non-zero entanglement growth from vacuum indicates that the cavity photon production and TLSs excitation is correlated. The Fano factor provides a more quantitative measure of the photon number variance than the Wigner function snapshots shown in Fig. 2c; these latter snapshots correspond to the instants when the Fano factor reaches its peak, subsequent trough, and long-time limit steady state. The photon production burst corresponds to the cavity mode Wigner function rapidly first spreading out and then forming a ring with width close to that of a coherent state, eventually settling into a thicker ring in the steady state due to environmental diffusion.

In order to get a more quantitative sense of the average cavity photon number dynamics scaling dependence on TLS number N , as well as model possible experimental set-ups, we must go to the large N_{crit} limit where it is not feasible to numerically solve the master equation (3). As an alternative, we can apply the approximate second order moment equations [14] that should become increasingly accurate in the large N limit, provided N is not too close to N_{crit} [18, 19], and which can be straightforwardly solved numerically for arbitrarily large N since the number of coupled moment equations is fixed and small.

We will assume in part the parameters of the 3D microwave cavity-coupled nitrogen vacancy (NV) center defect scheme of Refs. [21, 22], which observed signatures of Dicke superradiance. In particular, we consider a coupling strength $\lambda_0 = 2\pi \times 70$ mHz, corresponding to an NV defect coupling via its magnetic moment to the magnetic field component of the considered cavity electromagnetic vacuum mode with frequency $\omega_c = 2\pi \times 3.2$ GHz. Assuming a diamond membrane flexural oscillation amplitude $A = 10^{-10}$ m, the nonrelativistic coupling strength is $\lambda = \lambda_0 \omega_c A / (2c) \approx 1.5 \times 10^{-9}$ Hz. For the NV defects, the dominant relaxation process is through spin-phonon interactions with rate $\gamma_d \approx 2 \times 10^{-4}$ Hz [22]. On the other hand, assuming a realizable, superconducting microwave cavity quality factor $Q_c = 10^6$ [23], we have $\gamma_c = \omega_c / Q_c \approx 2 \times 10^4$ Hz. With these numbers, we have $N_{\text{crit}} = \gamma_c \gamma_d / (2\lambda)^2 \approx 4 \times 10^{17}$; the number N of microwave field-coupled defects in the experiment of Ref. [22] is in the range $(0.36 - 1.5) \times 10^{16}$, not far from the above N_{crit} value.

Figure 3a gives the first burst peak maximum and the long time limit steady state rescaled cavity photon numbers $\langle a^\dagger a \rangle / N$ dependence on N / N_{crit} . We observe clear evidence of a phase transition, with the slope of average photon number dependence on N changing sharply as N moves through N_{crit} . In particular, in the long time steady state, we obtain the following approximate analytical expressions well below and above N_{crit} , respectively [14]: $\langle a^\dagger a \rangle = \frac{N}{N_{\text{crit}}} \frac{\gamma_d}{\gamma_c + \gamma_d} \approx 2 \times 10^{-26} N \lll 1$ for $N \ll N_{\text{crit}}$, and $\langle a^\dagger a \rangle = N \gamma_d / (2\gamma_c) \approx 5 \times 10^{-9} N \ggg 1$ for $N \gg N_{\text{crit}}$; we can clearly see that the average cavity photon number generated from vacuum is negligible below and non-negligible above N_{crit} . While these steady state average photon numbers scale linearly with N , from Fig. 3b, we see that the first burst peak scales as N^α with $\alpha \approx 2$ for $N > N_{\text{crit}}$ (i.e., quadratically with N to a good approximation); the peak average photon number rapidly grows in magnitude relative to the steady state value with increasing N above N_{crit} . In Fig. 3c, we see that the delay

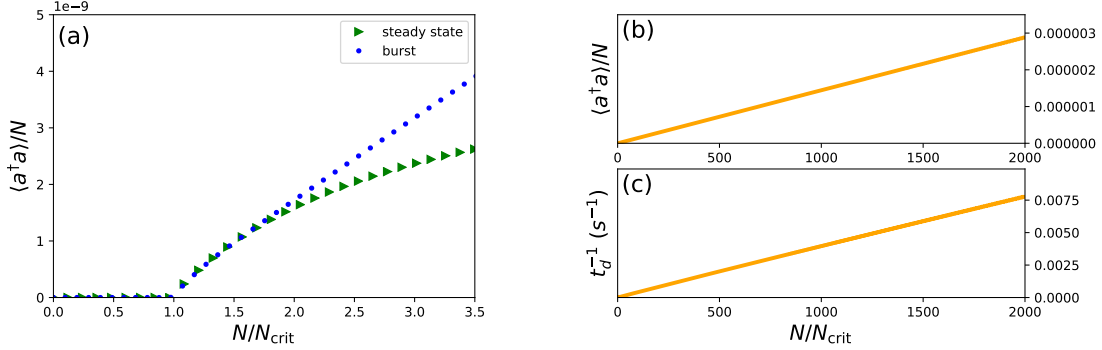


FIG. 3: (a) First burst peak value and long time limit steady state rescaled cavity photon numbers $\langle a^\dagger a \rangle / N$ versus N/N_{crit} . (b) First peak value of $\langle a^\dagger a \rangle / N$ and (c) first peak inverse delay time $1/t_d$ versus N/N_{crit} for $N \gg N_{\text{crit}}$. Assumed parameters are $\gamma_c \approx 2 \times 10^4$ Hz, $\gamma_d \approx 2 \times 10^{-4}$ Hz, and $N_{\text{crit}} \approx 4 \times 10^{17}$.

t_d in the appearance of this first burst peak starting from the initial cavity vacuum state becomes shorter as N increases, with the inverse delay scaling linearly with N .

These observed scaling dependencies for the first burst peak of photon production from vacuum coincide with those for Dicke superradiant bursts [22], however this is not properly a superradiant phase [19]. In order to understand better the nature of this enhanced oscillatory UE phase, apply the unitary transformation $U = \exp(i\pi J_x/2)$ to the master equation (3); the RWA Hamiltonian (2) transforms to the Tavis-Cummings Hamiltonian $H = \hbar\lambda(a^\dagger J^- + aJ^+)$, which involves co-rotating terms only, the Lindblad operators $\mathcal{L}_{\sigma_i^-}[\rho]$ are transformed to $\mathcal{L}_{\sigma_i^+}[\rho]$, and each TLS initial ground state is transformed to its corresponding excited state. The oscillatory UE cavity-TLSs system is thus unitarily equivalent to a Tavis-Cummings model with an incoherent pump. While the latter model does not exhibit a Dicke superradiant transition, which requires the presence of both co-rotating and counter-rotating terms of the Hamiltonian, it nevertheless exhibits a so-called lasing transition with the incoherent pump [19]. For this reason, the transition to an enhanced oscillatory UE may be thought of as a transition from a normal, incoherent phase below N_{crit} to a coherent inverted lasing phase above N_{crit} .

The challenge of any experimental scheme is to exceed the threshold for coherent photon production from vacuum (equivalently the inverted lasing threshold [19]), which in terms of the TLS number N is given by the condition $N > N_{\text{crit}} = \gamma_c \gamma_d / (2\lambda)^2$. In order to reduce the size of N_{crit} , we require microwave cavities with large quality factors, TLS's with small damping rates, and large TLS-photon coupling strengths λ_0 . One way to enhance λ_0 is to reduce the microwave cavity volume, for example by utilizing 2D coplanar microwave cavities [24–26]. However, this creates challenges for locating a sufficiently large number of TLS's within the microwave cavity region. On the other hand, while achievable λ_0 couplings for 3D microwave cavities are a few orders of magnitude smaller than what is possible for 2D coplanar cavities, correspondingly much greater numbers of TLS's can be located within the 3D microwave cavity region, furnished by defects within a flexurally vibrating membrane. The above mentioned NV centre scheme for probing Dicke superradiance [21, 22] is a promising direction, although larger cavity quality factors are required, as well as larger volume diamond membranes that can be actuated into GHz frequency flexural motion.

In conclusion, we have proposed a possible way to realize the actual oscillatory UE, where photons are produced from vacuum as a consequence of genuinely accelerating photodetectors. Our scheme involves a

membrane with a dense cloud of embedded NV defects (equivalently TLS photodetectors) undergoing driven, transverse flexural vibrations within a microwave cavity, and modelled as a driven Dicke-type Hamiltonian. When the resonance condition is satisfied, the system Hamiltonian simplifies via the RWA, thus allowing for an approximate analytical solution using the cumulant expansion approach. When the number N of TLS defects exceeds a critical value N_{crit} , the system undergoes a transition to an inverted lasing phase, signalled by a ‘burst’ peak in the average cavity photon number that scales as N^2 , yielding significantly enhanced, collective photon production from vacuum.

We thank A. D. Armour, W. F. Braasch, S.-Y. Lin, O. B. Wright, N. Shammah, A. R. H. Smith, and J. Yang for very helpful discussions. This work was supported by the NSF under grant no. DMR-1507383.

-
- [1] W. Unruh, Phys. Rev. D **14**, 870 (1976).
 - [2] M. O. Scully, V. V. Kocharovskiy, A. Belyanin, E. Fry, and F. Capasso, Phys. Rev. Lett. **91** 243004 (2003).
 - [3] J. Doukas, S.-Y. Lin, B. L. Hu, and R. Mann, J. High Energy Phys. **11**, 119 (2013).
 - [4] H. Wang, M. P. Blencowe, C. M. Wilson, and A. J. Rimberg, Phys. Rev. A **99**, 053833 (2019).
 - [5] M. P. Blencowe, and H. Wang, Phil. Trans. R. Soc. A. **378**, 20190224 (2020).
 - [6] P. D. Nation, J. R. Johansson, M. P. Blencowe, and F. Nori, Rev. Mod. Phys. **84**, 1 (2012).
 - [7] M. Sanz, W. Wiczczonek, S. Gröblacher, and E. Solano, Quantum **2**, 91 (2018).
 - [8] M. del Rey, D. Porras, and E. Martín-Martínez, Phys. Rev. A **85**, 022511 (2012).
 - [9] L. García-Álvarez, S. Felicetti, E. Rico, E. Solano, and C. Sabín, Sci. Rep. **7**, 657 (2017).
 - [10] R. H. Dicke, Phys. Rev. **93**, 99 (1954).
 - [11] M. Gross and S. Haroche, Phys. Rep. **93**, 301 (1982).
 - [12] V. M. Bastidas, C. Emary, B. Regler, and T. Brandes, Phys. Rev. Lett. **108** 043003 (2012).
 - [13] R. Chitra, and O. Zilberberg, Phys. Rev. A **92**, 023815 (2015).
 - [14] See Supplemental Material at XXX for further details.
 - [15] T. Holstein and H. Primakoff, Phys. Rev. **58**, 1098 (1949).
 - [16] J. R. Johansson, P. D. Nation, and F. Nori, Comput. Phys. Commun. **184**, 1234 (2013).
 - [17] N. Shammah, S. Ahmad, N. Lambert, S. D. Liberato, and F. Nori, Phys. Rev. A **98**, 063815 (2018).
 - [18] P. Kirton and J. Keeling, Phys. Rev. Lett. **118**, 123602 (2017).
 - [19] P. Kirton and J. Keeling, New J. Phys. **20**, 015009 (2018).
 - [20] G. Vidal and R. F. Werner, Phys. Rev. A **65**, 032314 (2002).
 - [21] A. Angerer, T. Astner, D. Wirtitsch, H. Sumiya, S. Onoda, J. Isoya, S. Putz, and J. Majer, Appl. Phys. Lett. **109**, 033508 (2016).
 - [22] A. Angerer, K. Streltsov, T. Astner, S. Putz, H. Sumiya, S. Onoda, J. Isoya, W. J. Munro, K. Nemoto, J. Schmiedmayer, and J. Majer, Nature Phys. **14**, 1168 (2018).
 - [23] M. Stammeier, S. Garcia, and A. Wallraff, Quantum Sci. Technol. **3**, 045007 (2018).
 - [24] M. Devoret, S. Girvin, and R. Schoelkopf, Ann. Phys. (Leipzig) **16**, 767 (2007).
 - [25] S. Probst, A. Bienfait, P. Campagne-Ibarcq, J. J. Pla, B. Albanese, J. F. Da Silva Barbosa, T. Schenkel, D. Vion, D. Esteve, K. Mølmer, J. J. L. Morton, R. Heeres, and P. Bertet, Appl. Phys. Lett. **111**, 202604 (2017).
 - [26] V. Ranjan, S. Probst, B. Albanese, T. Schenkel, D. Vion, D. Esteve, J. J. L. Morton, and P. Bertet, Appl. Phys. Lett. **116**, 184002 (2020).

Enhancing the oscillatory Unruh effect with a dense cloud of accelerating photodetectors: Supplemental material

Hui Wang¹ and Miles Blencowe¹

¹*Department of Physics and Astronomy, Dartmouth College, Hanover, New Hampshire 03755, USA*

In the following, we derive the RWA Hamiltonian (2) starting from the relativistic, parametrically driven Dicke model Hamiltonian (1). We then derive from the Lindblad master equation (3), approximate equations for the second moments of the cavity and TLSs degrees of freedom via a cumulant expansion.

DERIVATION OF THE RWA HAMILTONIAN

The single-mode, relativistic parametrically driven Dicke Hamiltonian (1) expressed in terms of J^z , J^\pm , and $\xi = \Omega_m A/c$ is

$$H = \hbar\omega_c a^\dagger a + \hbar\omega_{d0} \frac{d\tau}{dt} J^z + \hbar\lambda_0 \frac{d\tau}{dt} \sin \left[\frac{\omega_c \xi}{\Omega_m} \cos(\Omega_m t) \right] (\hat{a} + \hat{a}^\dagger) J^x, \quad (\text{S1})$$

where the reciprocal Lorentz factor $d\tau/dt = \sqrt{1 - \xi^2 \sin^2(\Omega_m t)}$ is the same for all detectors (TLSs) with the assumption that their phases $\phi_i = 0$. Applying the Fourier series expansion to $d\tau/dt$ and the Jacobi-Anger expansion to the $\sin[\omega_c \xi \cos(\Omega_m t)/\Omega_m]$ term, we obtain

$$\frac{d\tau}{dt} = \sum_{n=0}^{\infty} (-1)^n \binom{\frac{1}{2}}{n} \binom{2n}{n} \left(\frac{\xi}{2}\right)^{2n} + 2 \sum_{n=1}^{\infty} \sum_{n'=1}^n (-1)^{n-n'} \binom{\frac{1}{2}}{n} \binom{2n}{n-n'} \left(\frac{\xi}{2}\right)^{2n} \cos(2n'\Omega_m t), \quad (\text{S2})$$

$$\sin \left[\frac{\omega_c \xi}{\Omega_m} \cos(\Omega_m t) \right] = 2 \sum_{n=0}^{\infty} (-1)^n J_{2n+1} \left(\frac{\omega_c \xi}{\Omega_m} \right) \cos[(2n+1)\Omega_m t], \quad (\text{S3})$$

where the $J_{(2n+1)}(z)$ are Bessel functions of the first kind. Keeping only terms up to second harmonics in Ω_m , Eqs. (S2) and (S3) become approximately

$$\frac{d\tau}{dt} \approx D_0 + D_2 \cos(2\Omega_m t) \quad (\text{S4})$$

$$\frac{d\tau}{dt} \sin \left[\frac{\omega_c \xi}{\Omega_m} \cos(\Omega_m t) \right] \approx C_1 \cos(\Omega_m t), \quad (\text{S5})$$

where the ξ dependent D_0 and D_2 coefficients can be read off from Eq. (S2) and the ξ , Ω_m dependent coefficient $C_1 = 2J_1(\omega_c \xi/\Omega_m)$ can be read off from Eq. (S3). Substituting Eqs. (S4), (S5) into Hamiltonian Eq. (S1), we obtain

$$H = \hbar\omega_c a^\dagger a + \hbar[\omega_d + \omega_{d0} D_2 \cos(2\Omega_m t)] J^z + \hbar\lambda_0 C_1 \cos(\Omega_m t) (a^\dagger + a)(J^+ + J^-), \quad (\text{S6})$$

where $\omega_d = \omega_{d0} D_0$ is the renormalized detector oscillator frequency. Transforming to the rotating frame via the unitary operator $U_{\text{RF}}(t) = \exp(i\omega_c a^\dagger a t + iJ^z [\omega_d t + \omega_{d0} D_2 \sin(2\Omega_m t)/2\Omega_m])$, the cavity mode and detector annihilation operators pick up time-dependent phase terms as follows:

$$a(t) \rightarrow e^{-i\omega_c t} a(t),$$

$$\sigma_i^-(t) \rightarrow e^{-i\left[\omega_d t + \frac{\omega_{d0} D_2}{2\Omega_m} \sin(2\Omega_m t)\right]} \sigma_i^-(t). \quad (\text{S7})$$

The system Hamiltonian (S6) then becomes in the interaction picture:

$$H_I = \hbar\lambda_0 C_1 \cos(\Omega_m t) (e^{i\omega_c t} a^\dagger + e^{-i\omega_c t} a) \left[e^{i\omega_d t} e^{iB \sin(2\Omega_m t)} J^+ + e^{-i\omega_d t} e^{-iB \sin(2\Omega_m t)} J^- \right] \quad (\text{S8})$$

where $B = \omega_{d0} D_2 / 2\Omega_m < 1$.

Making use of the Jacobi-Anger expansion again such that

$$e^{\pm iB \sin(2\Omega_m t)} \approx J_0(B) \pm 2iJ_1(B) \sin(2\Omega_m t) \quad (\text{S9})$$

and substituting Eq. (S9) into Eq. (S8), we arrive at the following expression for the system Hamiltonian:

$$\begin{aligned} H_I \approx \hbar\lambda_0 C_1 \cos(\Omega_m t) & \left\{ e^{i(\omega_c + \omega_d)t} [J_0(B) + 2iJ_1(B) \sin(2\Omega_m t)] a^\dagger J^+ \right. \\ & + e^{-i(\omega_c + \omega_d)t} [J_0(B) - 2iJ_1(B) \sin(2\Omega_m t)] a J^- \\ & + e^{i(\omega_c - \omega_d)t} [J_0(B) - 2iJ_1(B) \sin(2\Omega_m t)] a^\dagger J^- \\ & \left. + e^{-i(\omega_c - \omega_d)t} [J_0(B) + 2iJ_1(B) \sin(2\Omega_m t)] a J^+ \right\}. \quad (\text{S10}) \end{aligned}$$

Imposing the parametric resonance condition $\Omega_m = \omega_c + \omega_d$ and combining the $\cos(\Omega_m t)$ term with the first two terms within the braces, we retain the time-independent terms and drop the oscillating terms at integer multiples of Ω_m (RWA). As a result, we recover the approximate time independent Hamiltonian (2):

$$H_I \approx \frac{\hbar\lambda_0 C_1}{2} [J_0(B) - J_1(B)] (a^\dagger J^+ + a J^-) = \hbar\lambda (a^\dagger J^+ + a J^-). \quad (\text{S11})$$

CUMULANT EXPANSION

We start from the dynamics of the cavity-TLS system, described by the Lindblad master equation:

$$\dot{\rho} = -\frac{i}{\hbar} [H, \rho] + \gamma_c \mathcal{L}_a[\rho] + \sum_{i=1}^N \gamma_d \mathcal{L}_{\sigma_i^-}[\rho], \quad (\text{S12})$$

where the Lindblad superoperators are defined by $\mathcal{L}_A[\rho] = A\rho A^\dagger - \frac{1}{2}A^\dagger A\rho - \frac{1}{2}\rho A^\dagger A$. Consider the unitary transformation $G = \exp[i\theta(a^\dagger a - J^z + N/2)]$, which leaves Hamiltonian (2) [(S11)] invariant. The master equation for the transformed system density matrix $\tilde{\rho} = G\rho G^\dagger$ is given by

$$\begin{aligned} \dot{\tilde{\rho}} &= -\frac{i}{\hbar} G[H, \rho]G^\dagger + \gamma_c G \mathcal{L}_a[\rho]G^\dagger + \gamma_d \sum_{i=1}^N G \mathcal{L}_{\sigma_i^-}[\rho]G^\dagger \\ &= -\frac{i}{\hbar} [H, \tilde{\rho}] + \gamma_c \mathcal{L}_a[\tilde{\rho}] + \gamma_d \sum_{i=1}^N \mathcal{L}_{\sigma_i^-}[\tilde{\rho}], \quad (\text{S13}) \end{aligned}$$

where we have applied the transformation relations $G^\dagger a G = e^{i\theta} a$ and $G^\dagger \sigma_i^- G = e^{-i\theta} \sigma_i^-$. Assume that the system state is initialized as a product state of the individual ground states of the isolated cavity and N isolated TLSs: $|\psi(0)\rangle = |0\rangle_c \otimes |-, -, \dots, -\rangle_s$. The fact that $\tilde{\rho}(0) = \rho(0)$ and the transformed equation (S13) coincides with Eq. (S12), indicates that $\tilde{\rho}(t) = \rho(t)$ for the whole time range; G is a symmetry of

the cavity-TLS system and initial state. As a consequence, only operators that are invariant under the G transformation give non-vanishing expectation values, and thus for the first and second moments, we need consider only the following non-zero terms: $\langle \sigma_1^z \rangle$, $\langle a^\dagger a \rangle$, $\langle a \sigma_1^- \rangle$, $\langle a^\dagger \sigma_1^+ \rangle$, and $\langle \sigma_1^+ \sigma_2^- \rangle$; all TLS's give the same moment values (a consequence of having the same assumed coupling and damping rates), which allows us to replace $\sigma_i^{z(+,-)}$ and $\sigma_i^+ \sigma_j^-$ ($i \neq j$) with $\sigma_1^{z(+,-)}$ and $\sigma_1^+ \sigma_2^-$, respectively. We have verified numerically for a few N TLSs using QuTiP [1] that the following noninvariant moments that would otherwise appear in the moment equations vanish: i.e., $\langle aa \rangle = \langle aJ^+ \rangle = \langle J^+ J^+ \rangle = 0$.

With Eq. (S12), the dynamical differential equations for the second moments can be obtained; these equations also include the nonvanishing third moment terms $\langle a^{(+)} \sigma_2^{-(+)} \sigma_1^z \rangle$ and $\langle a^\dagger a \sigma_1^z \rangle$. Rewriting σ_1^z through the identity $\sigma_1^z = 2\sigma_1^+ \sigma_1^- - 1$ and substituting into the third moments, we obtain the sum of a fourth moment term and one second moment term. By approximating the fourth moments through setting the fourth cumulants to zero, we obtain the following improved third-moment approximations:

$$\begin{aligned} \langle a \sigma_2^- \sigma_1^z \rangle &= \langle a \sigma_2^- \rangle \langle \sigma_1^z \rangle + 2 \langle a \sigma_1^- \rangle \langle \sigma_2^- \sigma_1^+ \rangle \\ \langle a^\dagger \sigma_2^+ \sigma_1^z \rangle &= \langle a^\dagger \sigma_2^+ \rangle \langle \sigma_1^z \rangle + 2 \langle a^\dagger \sigma_1^+ \rangle \langle \sigma_2^+ \sigma_1^- \rangle \\ \langle a^\dagger a \sigma_1^z \rangle &= \langle a^\dagger a \rangle \langle \sigma_1^z \rangle + 2 \langle a^\dagger \sigma_1^+ \rangle \langle a \sigma_1^- \rangle. \end{aligned} \quad (\text{S14})$$

The resulting approximate differential equations for the nonzero second moments and $\langle \sigma_1^z \rangle$ are

$$\begin{aligned} \frac{d}{dt} \langle a^\dagger a \rangle &= -\gamma_c \langle a^\dagger a \rangle - 2iN\lambda \langle a \sigma_1^- \rangle \\ \frac{d}{dt} \langle a \sigma_1^- \rangle &= -\frac{\gamma_c + \gamma_d}{2} \langle a \sigma_1^- \rangle - i\lambda \left[(N-1) \langle \sigma_1^+ \sigma_2^- \rangle - \langle a^\dagger a \rangle \langle \sigma_1^z \rangle - 2 \langle a \sigma_1^- \rangle \langle a^\dagger \sigma_1^+ \rangle + \frac{1 - \langle \sigma_1^z \rangle}{2} \right] \\ \frac{d}{dt} \langle a^\dagger \sigma_1^+ \rangle &= -\frac{\gamma_c + \gamma_d}{2} \langle a^\dagger \sigma_1^+ \rangle + i\lambda \left[(N-1) \langle \sigma_1^+ \sigma_2^- \rangle - \langle a^\dagger a \rangle \langle \sigma_1^z \rangle - 2 \langle a \sigma_1^- \rangle \langle a^\dagger \sigma_1^+ \rangle + \frac{1 - \langle \sigma_1^z \rangle}{2} \right] \\ \frac{d}{dt} \langle \sigma_1^+ \sigma_2^- \rangle &= -\gamma_d \langle \sigma_1^+ \sigma_2^- \rangle - 2i\lambda \left[\langle a \sigma_1^- \rangle \langle \sigma_1^z \rangle + 2 \langle a \sigma_1^- \rangle \langle \sigma_1^+ \sigma_2^- \rangle \right] \\ \frac{d}{dt} \langle \sigma_1^z \rangle &= -\gamma_d (\langle \sigma_1^z \rangle + 1) - 4i\lambda \langle a \sigma_1^- \rangle. \end{aligned} \quad (\text{S15})$$

The above nonlinear dynamical equations must be solved numerically, although an approximate analytical solution for the average cavity photon number can be obtained in the long time limit steady state, defined by setting to zero the time derivatives of the moments. In particular, we obtain $\langle a^\dagger a \rangle \approx N\gamma_d/(2\gamma_c)$ when $N \gg N_{\text{crit}}$, where $N_{\text{crit}} = \gamma_c \gamma_d / (4\lambda^2)$.

If we instead assume the usual, less accurate second moment approximation where the third order cumulants are set to zero, then the second terms on the right hand side of Eqs. (S14) are absent as well as the corresponding terms quadratic in the second moments in Eq. (S15). This then enables the following general analytic solution to be obtained for the average cavity photon number in the long time limit:

$$\langle a^\dagger a \rangle = \frac{N\gamma_d \{ (N - N_{\text{crit}})(\gamma_c + \gamma_d) - 2\gamma_c + \sqrt{(N - N_{\text{crit}})^2(\gamma_c + \gamma_d)^2 + 4\gamma_c [(N + N_{\text{crit}})(\gamma_c + \gamma_d) - \gamma_c]} \}}{4\gamma_c [N(\gamma_c + \gamma_d) - \gamma_c]} \quad (\text{S16})$$

In the limit $N, N_{\text{crit}} \gg 1$, Eq. (S16) simplifies approximately to

$$\langle a^\dagger a \rangle \approx \begin{cases} \frac{N\gamma_d}{N_{\text{crit}}(\gamma_c + \gamma_d)} & N \ll N_{\text{crit}} \\ \frac{N\gamma_d}{2\gamma_c} & N \gg N_{\text{crit}}. \end{cases} \quad (\text{S17})$$

While the more accurate, vanishing fourth cumulant approximation does not give a simple general analytic expression like Eq. (S16), it nevertheless yields the same approximate expressions as (S17) for $N, N_{\text{crit}} \gg 1$.

Note that the vanishing fourth cumulant approximation gives a more accurate approximation than the vanishing third cumulant approximation for the full dynamical evolution of the average cavity photon number, including the first burst peak dynamics.

[1] J. R. Johansson, P. D. Nation, and F. Nori, *Comput. Phys. Commun.***184**, 1234 (2013).